Solid State Laser Principles

Faranek Saboohi, Yinan Liu, Tolga Atalay
Department of Physics, Freie Universität Berlin

Abstract

Lasers are used in applications where high spatial and temporal accuracy is required. Diode pumped solid state lasers offer high slope efficiency, high beam quality in continuous operations and high peak power in Q-switched operations. In this experiment we demonstrate and characterize the continuous and Q-switched operations of diode pumped Nd:YAG laser and study the of non-linear optical materials to generate second harmonics. It is shown that second harmonics can be efficiently generated in Nd:YAG solid-state laser, peak power in Q-switched operation can exceed average power by orders of magnitude and experimental results are in a good agreement with theoretical expectations.

Theoretical Background

Light amplification by stimulated emission of radiation, also known as LASER, was first introduced in 1960 by American physicist Theodore Maiman[1]. Since this milestone in the history of optics, such system has been widely used in a variety of settings from medical to industrial and scientific applications. The basic ingredients for this remarkable tool include a pumping source, a gain medium, and an optical resonator.

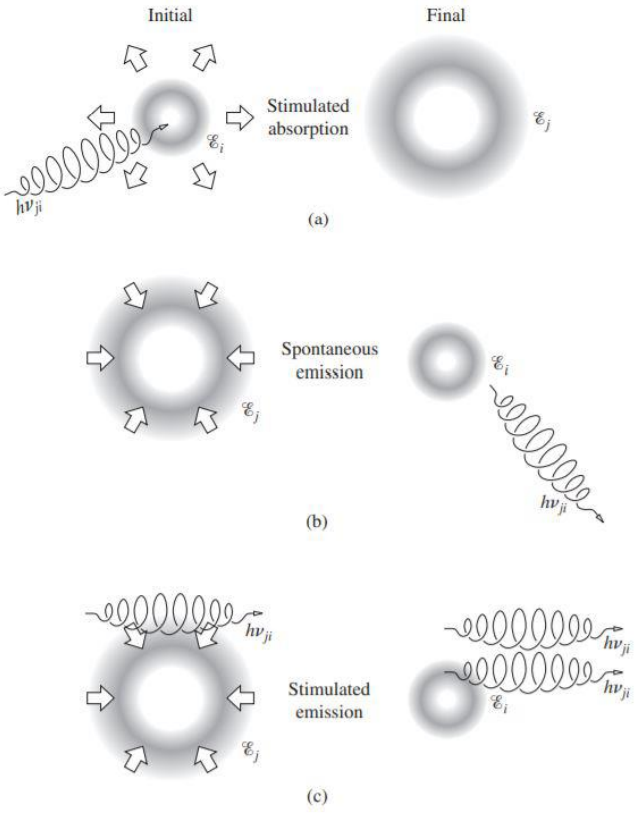

Figure 1: Schematics illustrating (a) stimulated absorption: photon is absorbed by an atom in its ground state, (b) spontaneous emission: the atom returns to its ground state and emits a photon, and (c) stimulated emission: a previously emitted photon leads an excited atom to emit an in-phase, coherent photon[1].

Light amplification in laser is achieved through energetic atoms in the pumping medium to reinforce the light field. Following the Maxwell-Boltzmann distribution, the population of the ith energy level is described by:

$$N_i = N_o e^{-\varepsilon_i / k_B T}$$

Eq. 1

where N_0 is constant at a given temperature. The radio between the population at the jth energy level where $\varepsilon_j > \varepsilon_i$ is given by:

$$\frac{N_i}{N_j} = \frac{N_o e^{-\varepsilon_i / k_B T}}{N_o e^{-\varepsilon_j / k_B T}}$$

Eq. 2

An atom can absorb energy and transition from its ground state to an allowable excited state if the absorbed energy is equal to the energy difference between the respective energy levels. If such a transition is coupled with the emission of a photon, then we have the following relationship between the energy difference of the two levels and the photon frequency:

$$\varepsilon_j - \varepsilon_i = h\nu_{ij}$$

Eq. 3

Since the configuration of an atom in an excited state is usually short lived, the atom in the excited state will return to its stable state and emit the energy difference as a photon. This process is also known as spontaneous emission. Additionally, an incident photon can interact with the atom in the excited state, allowing the release of its excess energy with the incoming photon. This process is known as simulated emission and its rate can be described by:

$$\frac{dN_j}{dt} = -B_{ji} N_j u_\nu$$

Eq. 4

Where B_{ji} is the proportionality constant for this process, also known as the Einstein coefficient, along with B_{ij} and A_{ji} for stimulated absorption and spontaneous emission, respectively. The lifetime of an excited state τ is inversely related to A_{ji}. At elevated temperatures, given the principle of detailed balance for a system under equilibrium, $B_{ij} = B_{ji}$. Therefore, the probability of stimulated emission is equal to the probability of stimulated absorption under such conditions[1].

Stimulated emission is responsible for the emitted photon in a laser system having the same frequency, polarization, and direction. According to the Boltzmann-Maxwell distribution, number of atoms in the ground state is greater than the number of atoms in the excited state. However, when a large of number of atoms are excited to the upper state, leaving it more populated than the ground state, population inversion is achieved, leaving the probability of simulated emission larger than absorption. An avalanche of stimulated emission can then be initiated by a photon of proper frequency. Each photon induces another atom to emit photons with the same frequency and polarization that propagate in the same direction. Meanwhile, pumping is used to maintain the population inversion.

Consider the first pulsed ruby laser from Hecht as an example of a three-level active medium[1]. Optical pumping was given by a discharge lamp for the first ruby laser's active medium, an Al_2O_3 crystal containing roughly 0.05 (by weight) Cr_2O_3. Figure.2 shows the

ruby laser's energy levels. The absorption bands of Cr^{3+} ions are illustrated in this picture. The excited ions relax non-radiatively into the metastable state very quickly (in around 100 ns). Mechanical interactions such as collisions cause non-radiative relaxation, which produces no photons. In the lattice, phonon vibrations carry energy differences between layers. Up to several ms[1] is the metastable state's room temperature lifespan. atoms shift to the ground state by stimulated emission when population inversion is achieved A red laser beam with a λ of 694:3 exits the partially transparent side of the resonator in this process.

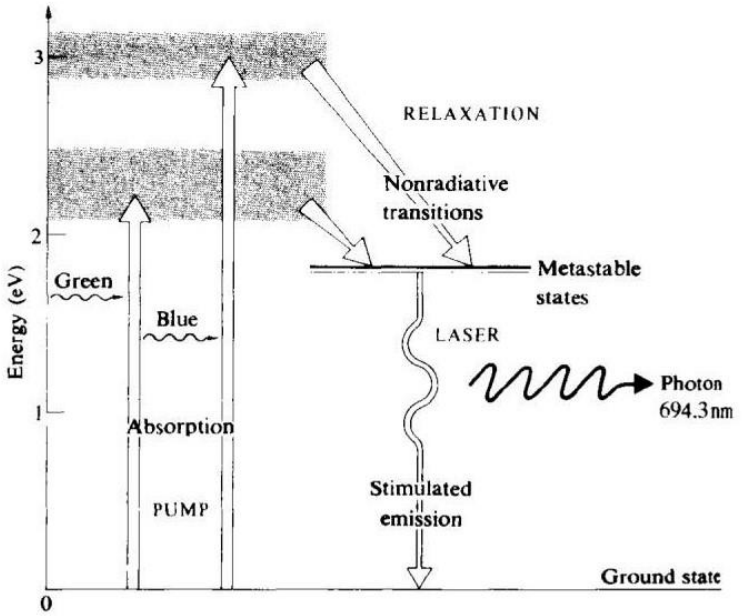

Figure 2: Ruby laser's three levels. Atoms are accelerated to the absorption band. They rapidly decompress to a meta stable state via a radiation-less transition. Stimulated emission liberates the laser frequency photons.[1]

An optical cavity or resonator is formed by placing an active medium between two parallel mirrors which trap the emission in specific modes. One of the mirrors in the optical cavity has a slightly lower reflectivity that allows a small amount of emission to escape[2]. Radiation is reflected back at the mirrors and into the active medium within the cavity. Numerous such round trips result in a rise in stimulated emission, which results in an increase in photon power. Through stimulated emission, photons lost due to various reasons such as mirror transmission and diffraction can be compensated. When stimulated emission outperforms spontaneous emission, the lasing threshold is attained.

Oscillating modes within the cavity are determined by the dimensions of the cavity. Some modes may not be able to survive in the active medium, resulting in an inhomogeneous gain profile. Figure.2 depicts the inhomogeneous gain curve and cavity modes.

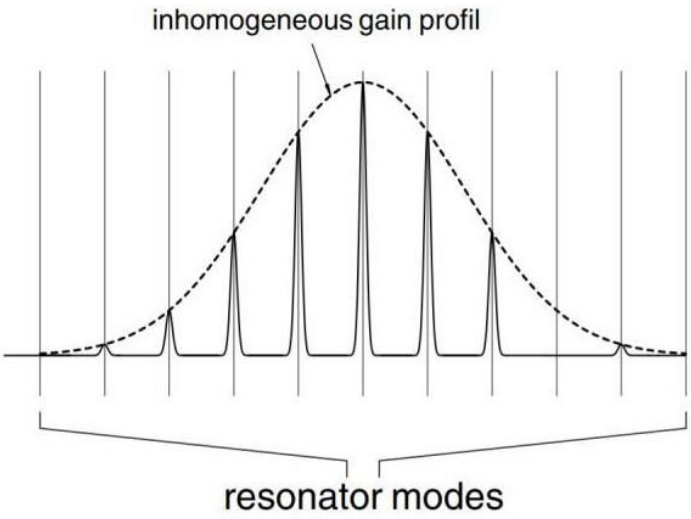

Figure 2: Profile with inhomogeneous gain (dotted curve) and resonator modes. The bandwidth of the dotted gain is compared to that of the cavity modes.[2]

Standing waves with nodes in the axial direction of the resonator are formed by photons traveling in a round-trip path along the cavity's longitudinal mode. As a result, one can compose:

$$2L = m\lambda = \frac{m\vartheta}{v}$$

Eq. 5

$$v = \frac{m\vartheta}{2L}$$

Eq. 6

where m is the number of nodes and v denotes the frequency. Cavity modes are then classified according to:

$$\delta v = \frac{\vartheta}{2L}$$

Eq. 7

The boundary conditions on waveguide edges, or in this case, on electromagnetic wave cavity mirrors, produce discrete transverse modes designated by TEM_{nm}, where n and m denote the total number of intensity dots minus one along the x and y axes, respectively (Figure 3). These parameters are usually adjusted to meet the stability criterion of the optical cavity, which describes the maximum length of the cavity at which it is able to contain the radiation.

$$0 \leq (1 - \frac{L}{R_1})(1 - \frac{L}{R_2}) \leq 1$$

Eq. 8

TME_{00} is a cross-section-free Gaussian flux density, and is most widely used. For nodes showing cylindrical or cartesian symmetry, a two-dimensional Laguerre-Gaussian and Hermite-Gaussian polynomials can be fitted accordingly.

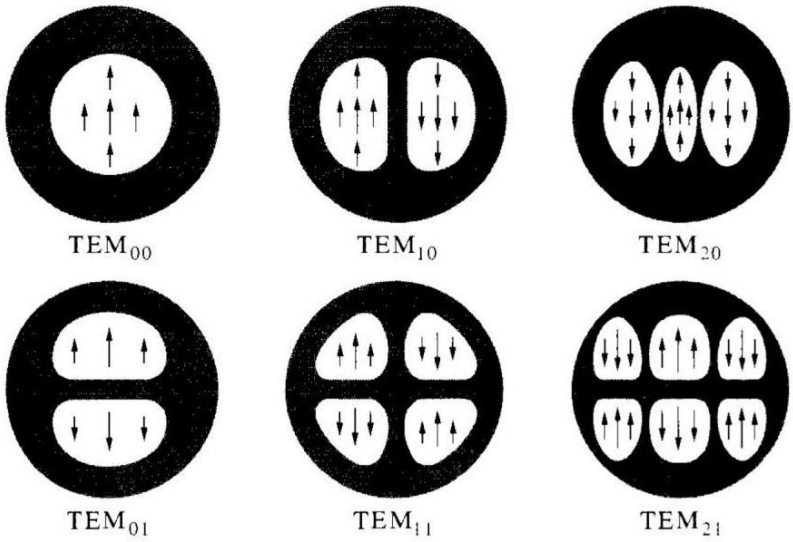

Figure.3: A rectangular cavity has several transverse modes. The white spots reflect more light, while the arrows indicate the direction of the electric field.[1]

Cavities come in a variety of shapes and sizes, including Fabry Perot cavities with two planar mirrors, two spherical mirrors, or one spherical and one planar mirror. The first resonator is difficult to modify, while the second resonator produces undesirable transverse modes despite its ease of adjustment. The most convenient type is composed of one planar element and one spherical element, which is also utilized in the Nd:YAG laser.

Nd:YAG laser

Solid-state materials have several advantages as an active medium in laser when compared to other choises such gases in liquids. Since Maiman's first solid state laser using ruby crystal, neodymium-doped aluminum-yttrium garnet (Nd:YAG) has become one of the most common laser media. It is a four-level medium that has four discrete absorption bands between $^4I_{9/2}$, to $^4F_{5/2}$(Figure 1) arising from the electronic states of Nd^{3+} ions in the $Y_3Al_5O_{12}$ host crystal[2]. The wavelengths associated with these bands take place between 804.4 and 817.3 nm. Absorption promotes electrons from the $^4I_{9/2}$ energy level to one of two unstable sublevels of $^4F_{5/2}$. Through the non-radiative coupling with lattice phonons, which are quasi particles of lattice vibrations, the system is transferred from $^4F_{5/2}$ to one of two metastable sublevels of $^4F_{3/2}$. Lasing transitions to the $^4I_{13/2}$, $^4I_{11/2}$, and $^4I_{9/2}$ occur from here, emitting light with wavelengths of 946, 1064, and 1322 nm.

Higher slope efficiency (the ratio of output laser emission power to input pumping power) and higher quantum yield (the fraction of absorption photons that contribute to electron excitation at a higher level of the lasing transition) are the results of the excited $^4F_{3/2}$ state having a long lifetime, and the fast non-radiative transition between $^4F_{5/2}$ and $^4F_{3/2}$.

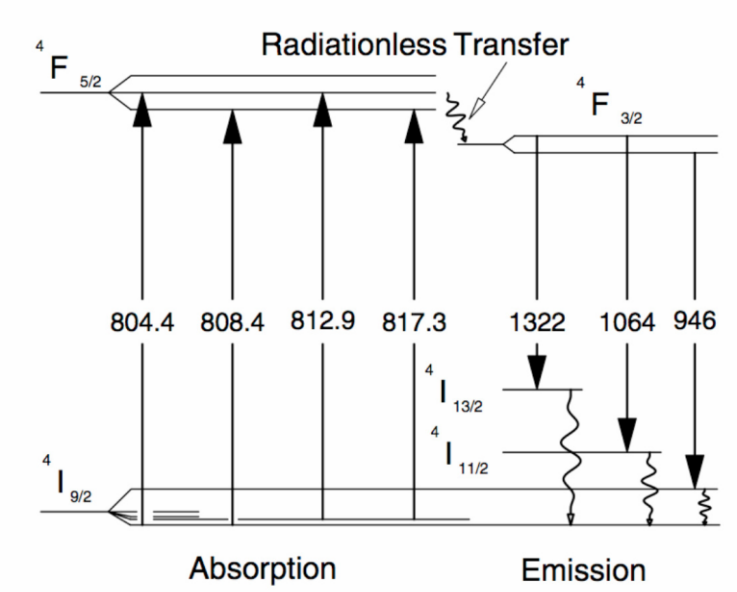

Figure 4. Term scheme for the Nd:YAG medium with its four-levels for lasing [2].

Pumping Photodiode

A diode laser is utilized to generate electronic excitations in the Nd:YAG active medium. This is preferred over the more economical flash or arc lamps because of its efficiency and stability. Diode laser is made from a pn-junction semiconductor. In our experiment, p and n-doped AlGaAs is used with an GaAs zone in in between the p and n doped layers (Figure 4).

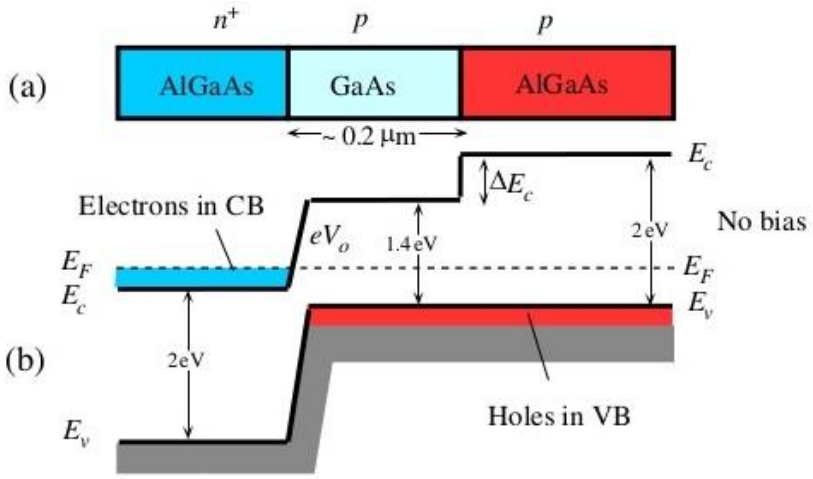

Figure 5. AlGaAs photodiode band diagram. E_c and E_v denote the energies at the conduction band's bottom and valence band's top, respectively, whereas E_F denotes the Fermi energy [3].

When materials come into contact, their Fermi levels become constant throughout the junction. At any point in time, the Fermi level is the energy level where the probability of detecting an electron is equal to 1/2. The location of this level within the band structure is critical in determining the material's electric characteristics. This alignment of the Fermi levels results in the formation of a depletion zone in the region between p- and n-type semiconductors, where the positive and negative ions from each side generate a space charge separation that prevents electrons and holes from passing through. For example, a big enough

forward bias can cause holes and electrons from both regions to merge together in the depletion zone, producing photons with an energy equal to the bandgap energy E_g.

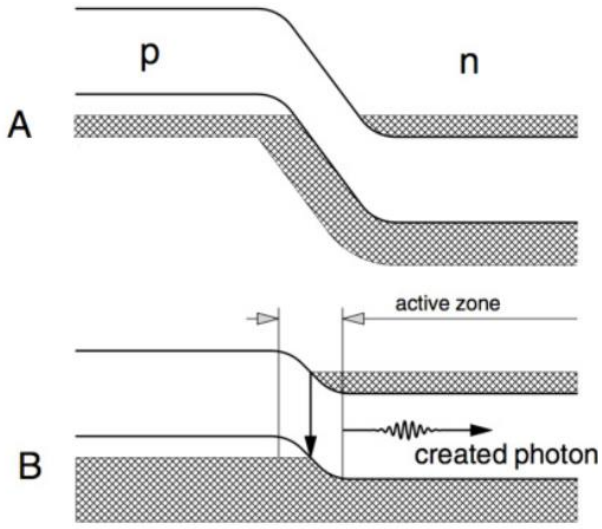

Figure 6.: Energy diagrams of a photodiode without an applied voltage (A) and with forward bias emitting radiation due to electron-hole recombination (B). Source of the illustration:[4]

Due to the refractive indices of the p- and n- semiconductors at a particular wavelength, the junction acts as a waveguide and the lased photons propagate parallel to it. By adjusting the applied current and/or the diode's temperature, photodiodes can be controlled to produce light of various wavelengths. The bandgap energy is also temperature dependent. Therefore, it is probable that increased carrier concentrations in the active region of the LED affect the bandgap energy, and clearly, increased forward bias, i.e. increased current, increases carrier concentrations. As a result, precise experiment control is needed to meet pumping stability.

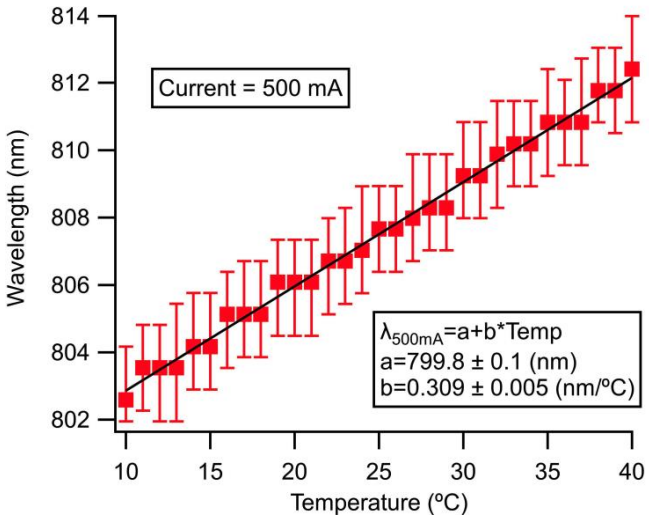

Figure 7. Temperature dependence of photodiode wavelength [2].

Q-Switching and Mode Locking

When great time resolution or a high peak power or intensity are required, a pulsed laser is the natural choice. It produces a pulsed discharge rather than a continuous discharge. Q-switching can be used to develop such a lasing system. The optical resonator's quality factor, or Q-factor, which describes the cavity's "underdampedness," is reduced to halt the lasing process before being rapidly increased. This enables the stimulation of a greater population of laser-active ions, resulting in the generation of a more intense pulse. Another technique is mode locking, which involves phase locking multiple distinct longitudinal modes so that their linear combination produces an incredibly brief pulse.

Pockels cells are frequently utilized to implement Q-switching. A Pockels cell is essentially a wave plate with a birefringence that is proportional to either the applied voltage V (the Pockels effect) or to V^2 (the Kerr effect). Birefringence is a feature of certain materials, particularly crystals, in which the refractive index of a beam of light is direction and polarization dependant. For example, when a certain voltage is provided, a Pockels cell can be set to rotate polarization 90 degrees, acting as an on-off switch for incident polarized light when paired with a polarizer [2].

Another optoelectronic device that is employed in Q-switching is an optoacoustic modulator. A piezoelectric element is linked to a transparent medium and can be vibrated, often in the radio frequency range, to generate audible vibrations. Sound waves appear to light travelling through a medium as planar fluctuations in material density, and consequently in refractive index. As these planes are evenly distributed across the sample, this results in scattering and/or diffraction.

Gain bandwidth is the width of the active medium's lasing transition's spectral line. Active media with wider gain bandwidth lend themselves more readily to the construction of brief pulses because they provide more frequencies to work with during mode locking. Recall how a particular waveform can be built from a sum of sinusoids via Fourier analysis. In another manner, this comes from the time-bandwidth product's minimal value.

The time-bandwidth product is the product of the laser pulse's time duration and spectral width. There is always a minimum value associated with this product. For example, it is 0.44 for the full-width half-maxima of Gaussian peaks. This relationship arises as a result of the Fourier transform, which converts a function between the time and frequency domains:

$$F(\omega) = F\{f(t)\}(\omega) = \int_{-\infty}^{\infty} dt\, e^{i\omega t}.f(t)$$

Eq. 9

Mode locking can be regulated externally by adjustable optoacoustic modulators (active mode locking) or it can be self-modulated via Kerr lenses or saturable absorbers (passive mode-locking). This enables the laser pulses to be aimed. A saturable absorber is a substance that absorbs more efficiently when exposed to weaker light sources. Additionally, self-modulation is possible via colliding-pulse mode locking. This is a technique that involves the interaction of two pulses traveling in opposite directions in a saturable absorber. Coherent sidebands will arise when the cavity is modulated at a frequency v_{mod} mod considerably less than v . At $v \pm v_{mod}$ mod, these are distinct sidebands, where v_{mod} mod is the cavity's modulation frequency. The time it takes for light to roundtrip in cavity is related to the cavity's modulation frequency by $\tau_{rep} = 1/v_{mod}$.

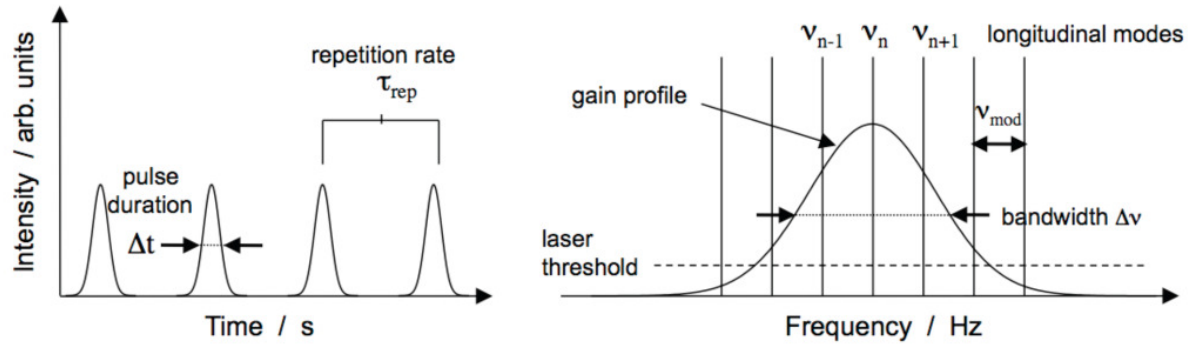

Figure 8. Schematics illustrating principles of mode locking [2].

Following the theoretical relationship, for the Ng:YAG laser, its emission at v=282 THz and 1064 nm correlates to a gain bandwidth of 0.12 THz and a minimum pulse duration of 3.7ps. Although the shortest pulse duration has been only reported at around 9ps, and the pulses commonly lies in the nanosecond to the lower microsecond range.

Nonlinearity and Second Harmonic Generation

The field of nonlinear optics probe how intense light interacts with matter. The process of frequency doubling, also known as second harmonic generation in non-centrosymmetric crystals provides an introductory example to nonlinear optics.

Without inversion symmetry, crystal materials can display nonlinearity, in which an input (pump) wave can generates another wave with double the optical frequency in the medium[4]. The pump wave is typically given using a laser beam, while the frequency-doubled (second-harmonic) wave is generated via a beam moving in the same direction (Figure 9).

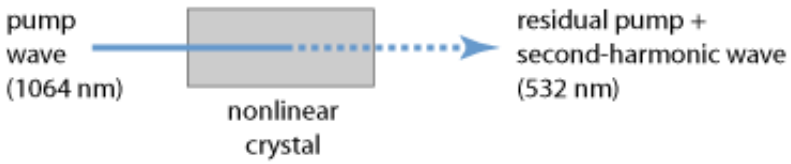

Figure 9.: A common frequency doubling configuration: an infrared input beam at 1064 nm yields a green 532 nm wave as it passes through a nonlinear crystal [5].

Frequency doubling requires the conservation of energy and momentum. The most common technique employed in meeting the phase matching condition is through using the birefringence of a biaxial crystal. The angle between the optical axis and the incoming wavevector where the phase matching condition is satisfied is known as the phase-matching angle θ [6].

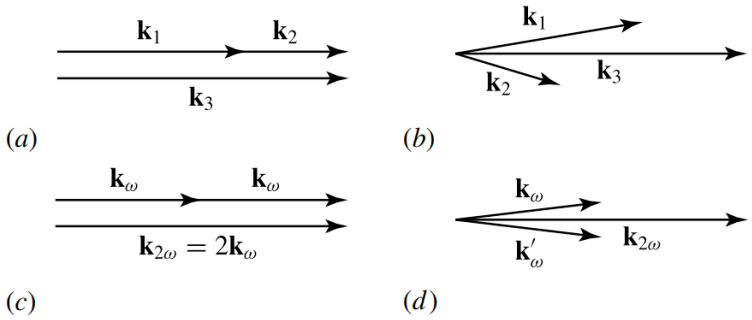

Figure 10. Colinear (a) and non-colinear(b) phase matching for a second order process with condition k3=k1+k2. Colinear (c) and non-colinear (d) phase matching for second order harmonic generation [6].

When the second-harmonic intensity develops, the latter interacts with the fundamental wave, allowing the pump wave to be attenuated (pump depletion): energy is transferred from the pump wave to the second-harmonic wave[5]. Because the efficiency of second harmonic conversion is low at low pump intensities and increases linearly with rising pump intensity, the intensity of the second harmonic (frequency-doubled) wave grows in lockstep with the pump intensity:

$$P_2 = \gamma P_1^2$$

Eq. 10

In this case, factor γ is determined by a variety of crystal parameters, including effective mode area, crystal length, and effective nonlinearity.

Experimental Setup

Schematic of experimental setup shown in Fig. 11 and corresponding equipment list depicted in Table 1 are taken from the laboratory manual [2].

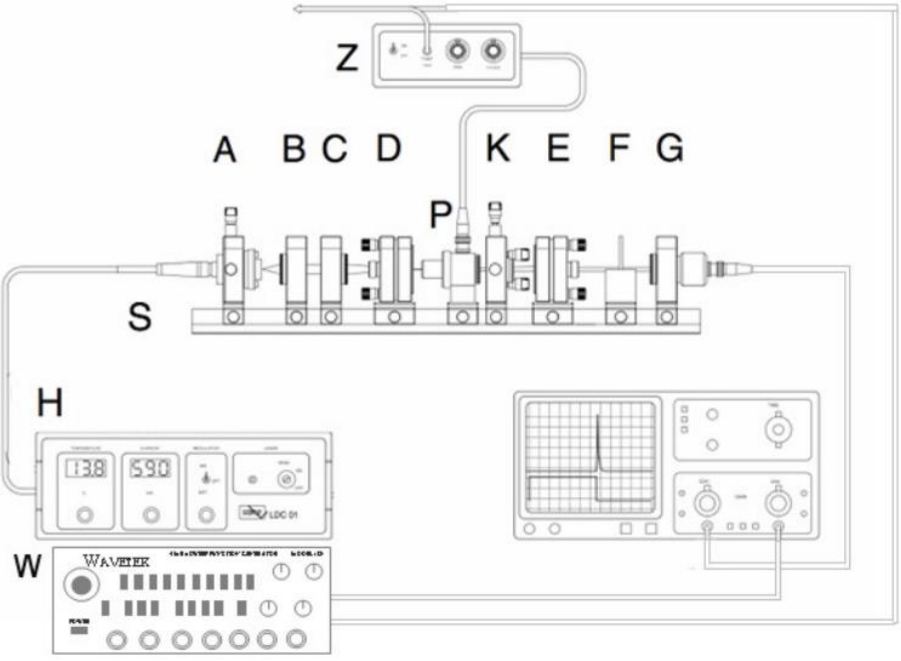

Figure 11. Experiment with a Q-switched Nd:YAG laser equipped with intracavity second harmonic production [2].

	Device	Note to the Function
A	Diode pump laser	with current and temperature controller (H)
B	Telescope lens	collimator for the laser diode emission
C	Telescope lens	focusing of the laser diode emission
D	End mirror/Nd:YAG medium	coated for 532 and 1064 nm operation
E	Output coupler	with mirrors for 532 and 1064 nm operation
F	Filter holder	for high/low pass and gray filters + CMOS chip
G	Photodiode	relative measurements of the laser output power
K	Second harmonic unit	KTP crystal in a mount for angle adjustments
P	Pockels cell	Q-switch with high-voltage supply (Z)
O	Oscilloscope	readout of the photodiode
S	Slide rail	for optical mounts at variable distances
W	Frequency generator	to trigger the Pockels cell

Table 1. Chart of experimental equipment for figure 11 [2].

Experimental procedure and results

The experiment was started by setting up all the component of our laser system according to figure 11. We first started optimizing the power output through maneuvering the focusing lens of the diode laser. After the system is collimated and optimized for lasing, power of the pump diode as a function of diode current is recorded with power meter and shown in Figure 12. A number of 23 data points were taken from 500mA to 160mA diode current. Temperature is varied according to the spectral calibration curve for emission at 808.4 nm.

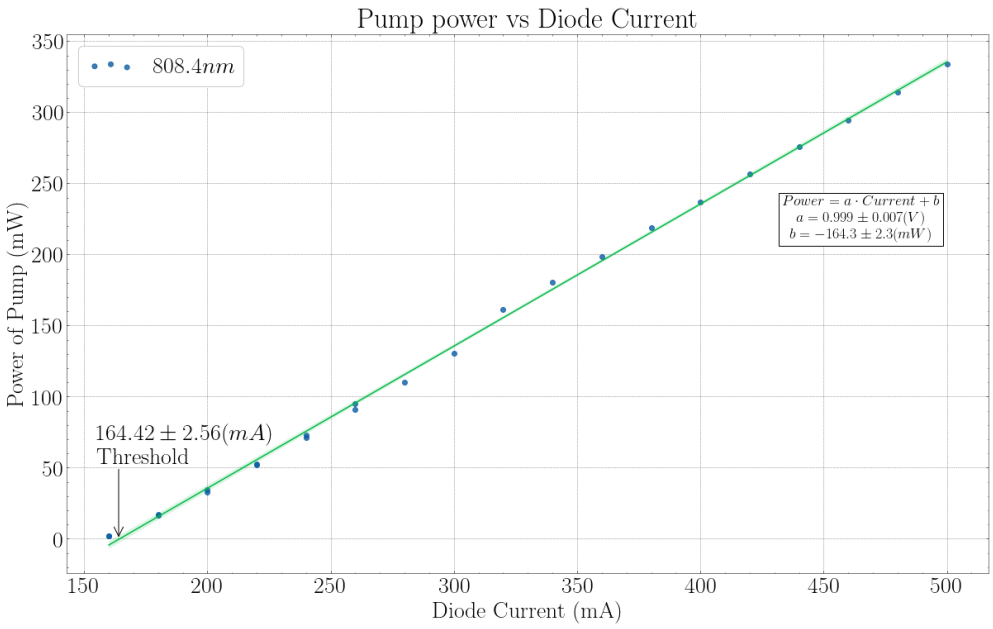

Figure 12. Pump power as a function of diode current calibrated for emission at 808.4 nm.

Then the optical resonators for the Nd:YAG laser was set up. The stability criterion for the two mirrors was calculated according to equation 8 and determined to be 10cm. Resonator mirrors of the Nd:YAG laser were adjusted in their distance and angles to optimize the power output. To block residual pump laser, a low-pass edge filter is used. The maximum power we have achieved prior to starting the experiment was at 16.49 mW.

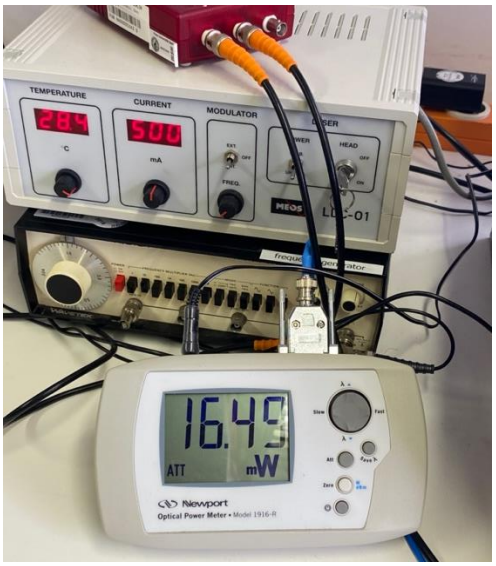

Figure 13. From top to bottom: Modulator for diode laser pump, frequency generator for the Nd: YAG laser, and power meter monitor.

Using the calibration results of the diode laser from the first task, we are then interested in seeing how the output power of the Nd:YAG laser changes when adjusting the power of the diode laser. Output power of the Nd:YAG laser as a function of diode pump power is recorded and shown in figure 14.

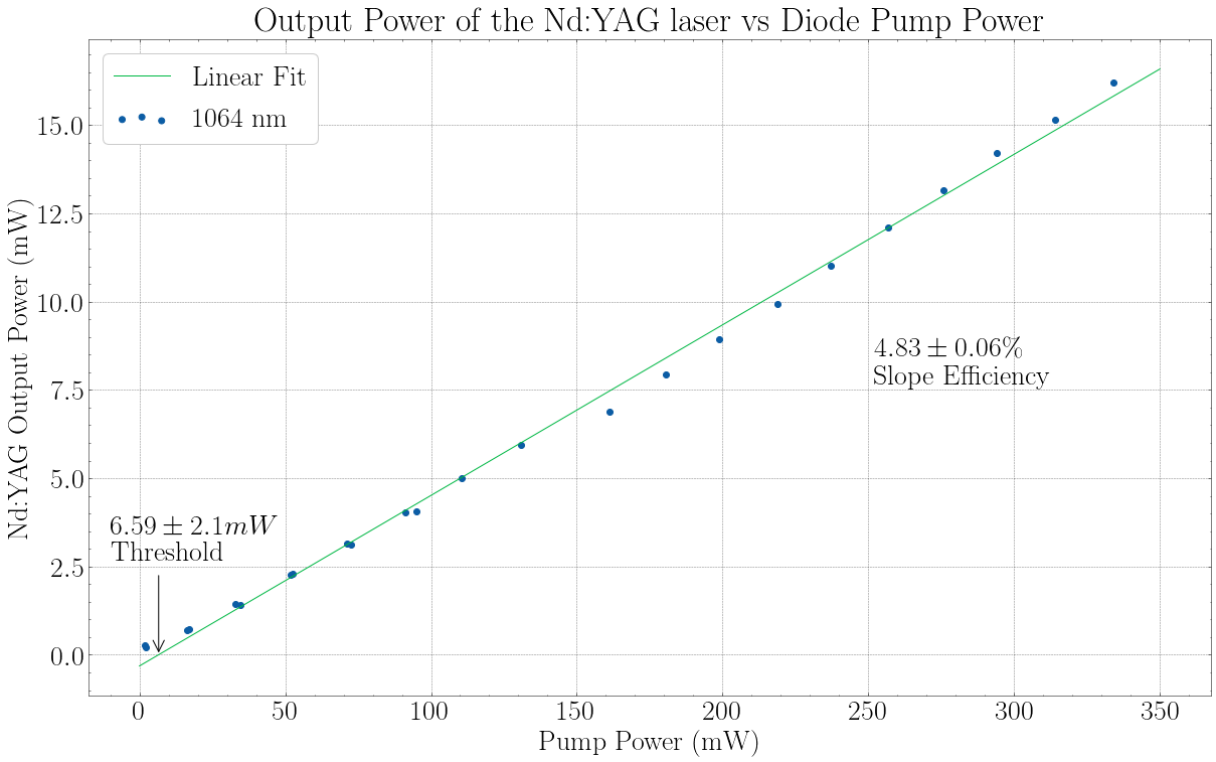

Figure 14. Nd:YAG output power as a function of pump power.

Figure 13 shows roughly linear relation between lasing power and pump power above 30 mW, and a threshold pump power of 6.59 mW. Applying a linear regression fit through all the data points, we arrive at a 4.83% slope efficiency of our system.

Next, maintaining a constant diode current at 500mA, we recorded output power of the Nd:YAG laser as we varied diode temperature from 10 to 40 degree Celsius (Figure 15).

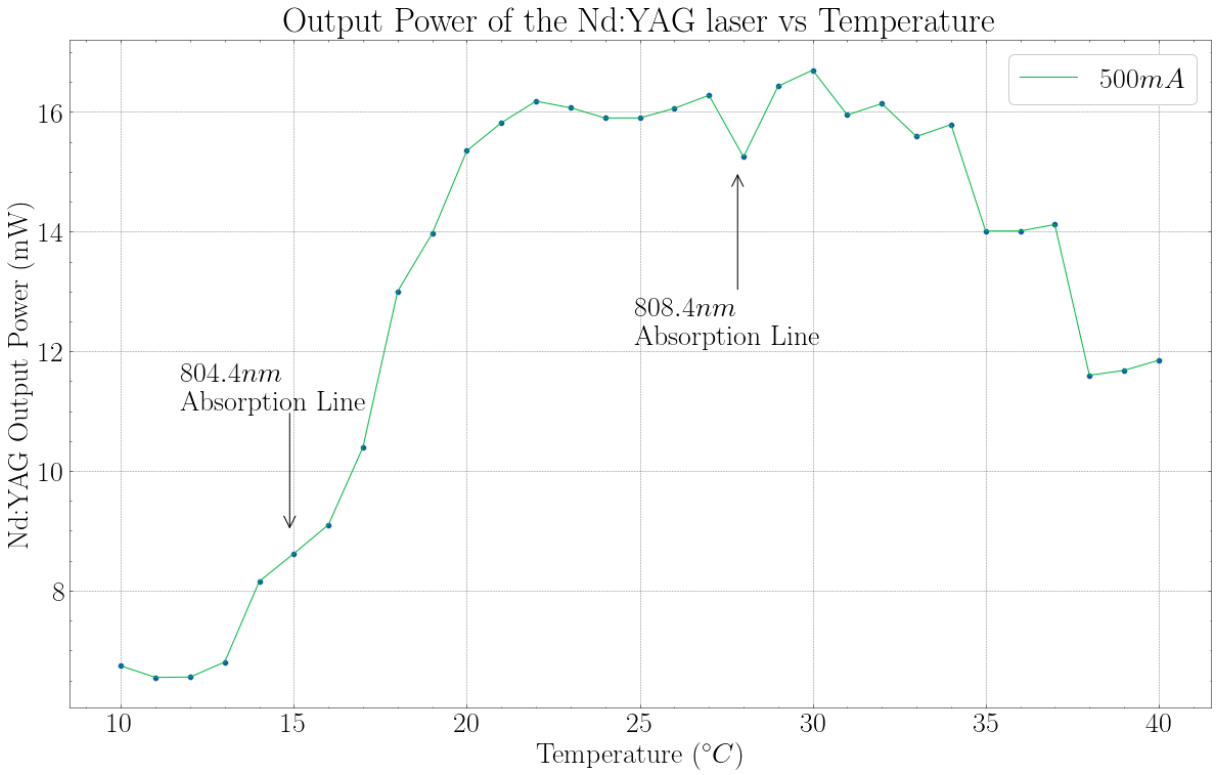

Figure.15: Temperature dependence of Nd:YAG output power at constant current of 500mA.

A KTP crystal is then inserted into the optical cavity close to the Nd:YAG medium to observe the generation of second harmonics. Lasing output for 532 nm emission is optimized by adjusting the cavity mirrors again and the angle of the KTP crystal. The low pass band filter is replaced with the high pass band filter. The output power at 532nm is recorded as we varied the diode modulator according to the calibration curve of the diode laser. A graph of second harmonic power as a function of pump power is plotted in figure 16.

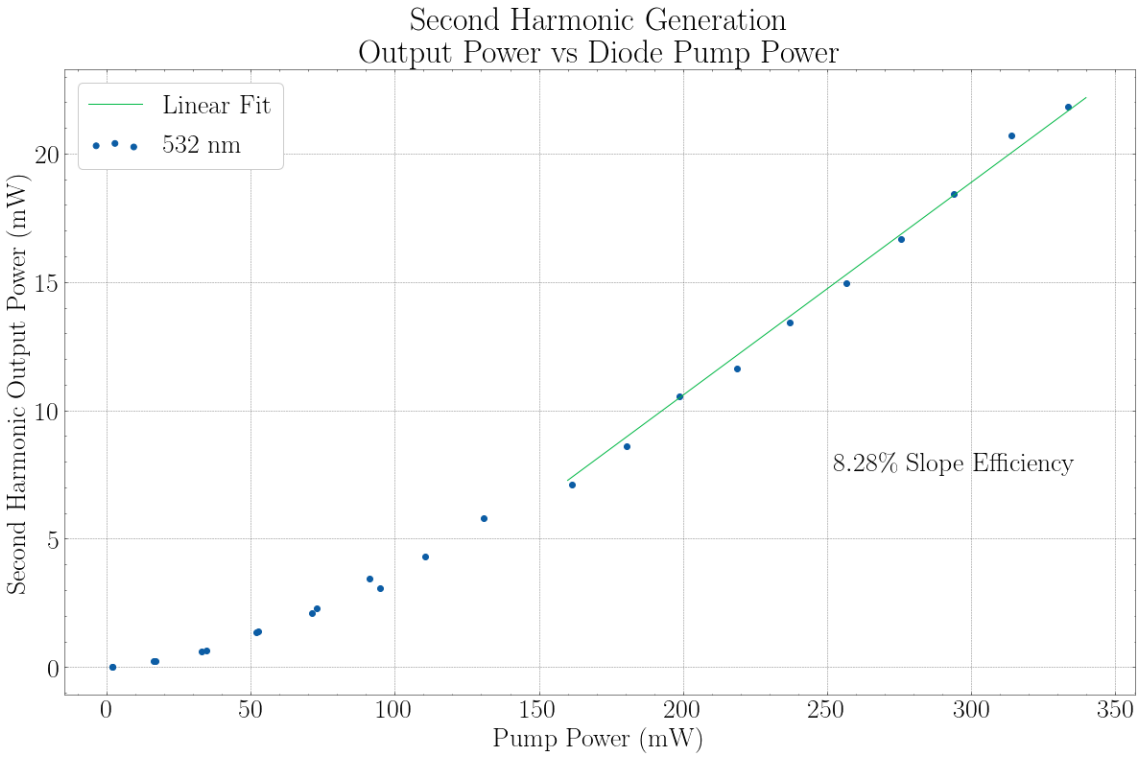

Figure.16: Second harmonic wave power as a function of pump power when KTP is near Nd:YAG medium.

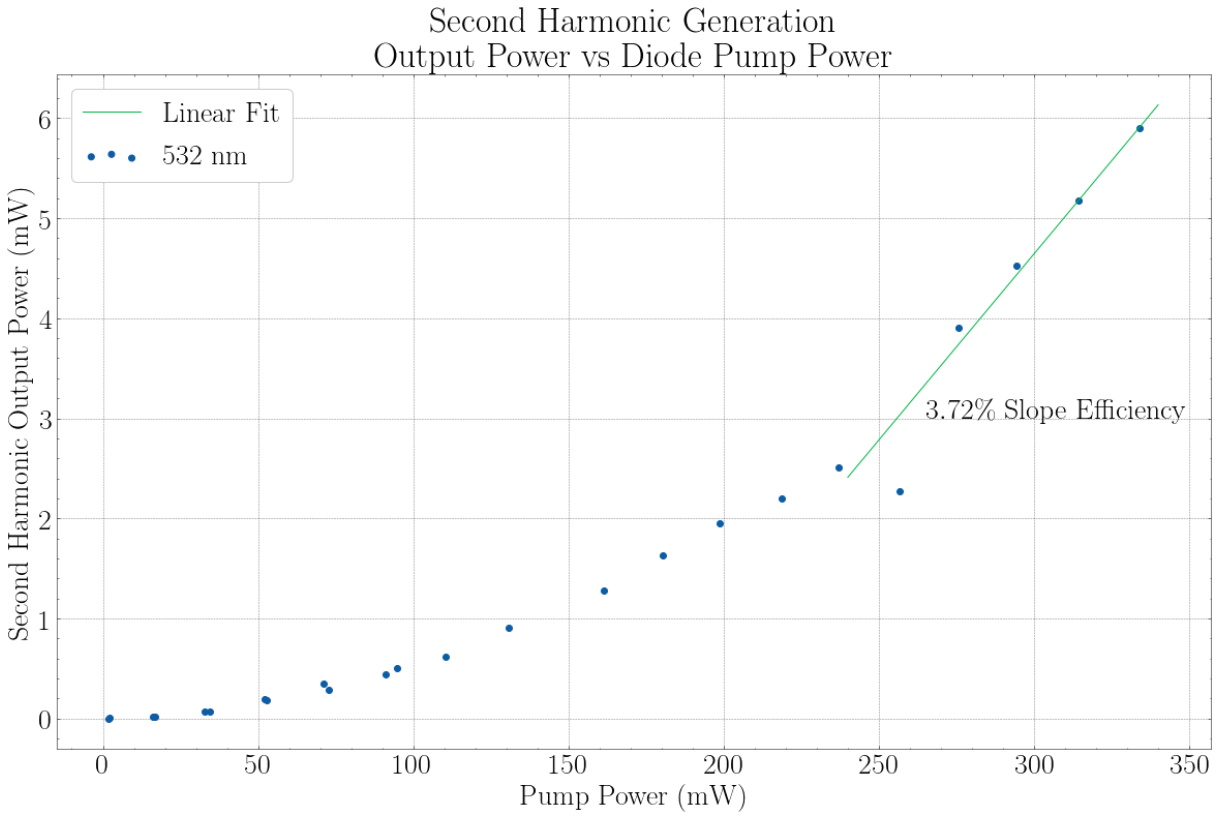

Figure.17: Second harmonic wave power as a function of pump power when KTP is near output mirror..

A linear regression line is fitted for data points larger than 150mW pump power to arrive at a slope efficiency at 8.28%.

The KTP crystal is then moved to the far side close to the out mirror. The same recording was done to document output power as a function of diode power (Figure 17).

Then, KTP crystal is moved back to the near position close to the Nd:YAG medium, and a Pockels cell is inserted into the optical cavity. The Pockels cell is rotated until maxmum lasing is achieved at 532nm. The Pockels cell controller and a PC output is turned on to observe laser pulse at varying frequencies from 1-50 Hz. A PC output is turned on to record the data from an oscilloscope at around 100, 250, and 400 Hz on the controller. Pulse train of Q-switched Nd:YAG laser is characterized, and power meter is used to measure average power of Q-switched Nd:YAG lasing. Figure 19, 20, and 21 shows single pulse (a) and pulse train (b) for the three frequencies.

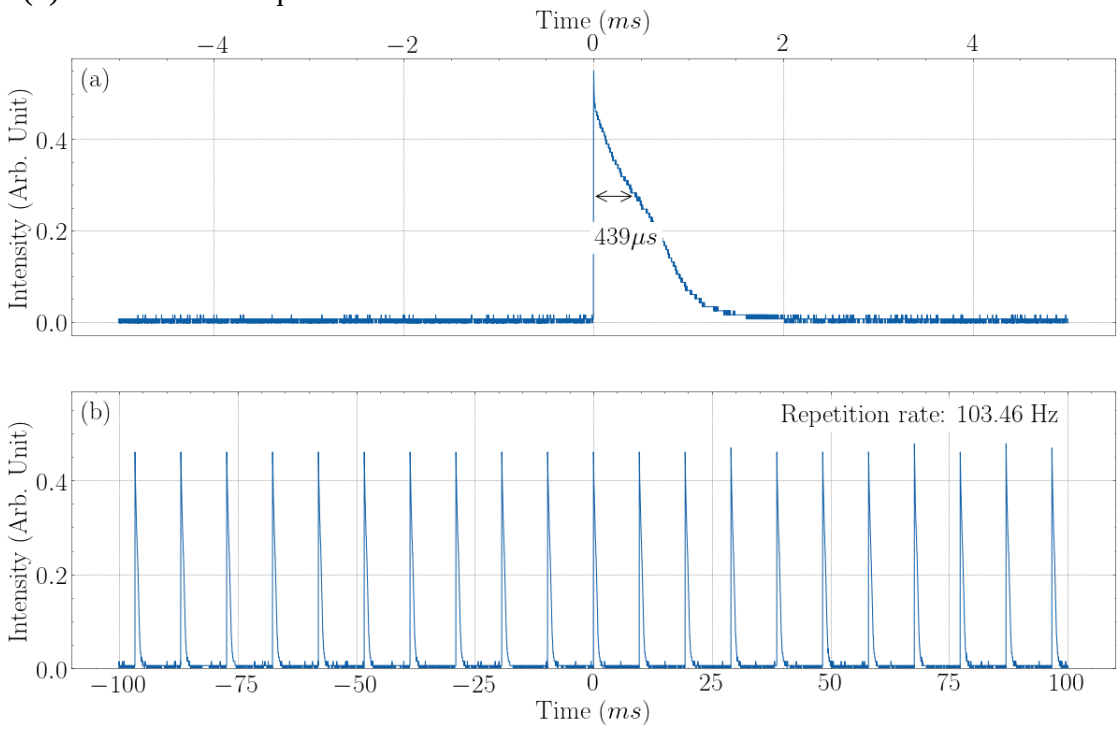

Figure 18. (a) Single Q-switched Nd:YAG laser pulse. (b) pulse train of Q-switched Nd:YAG laser at 103.46 Hz..

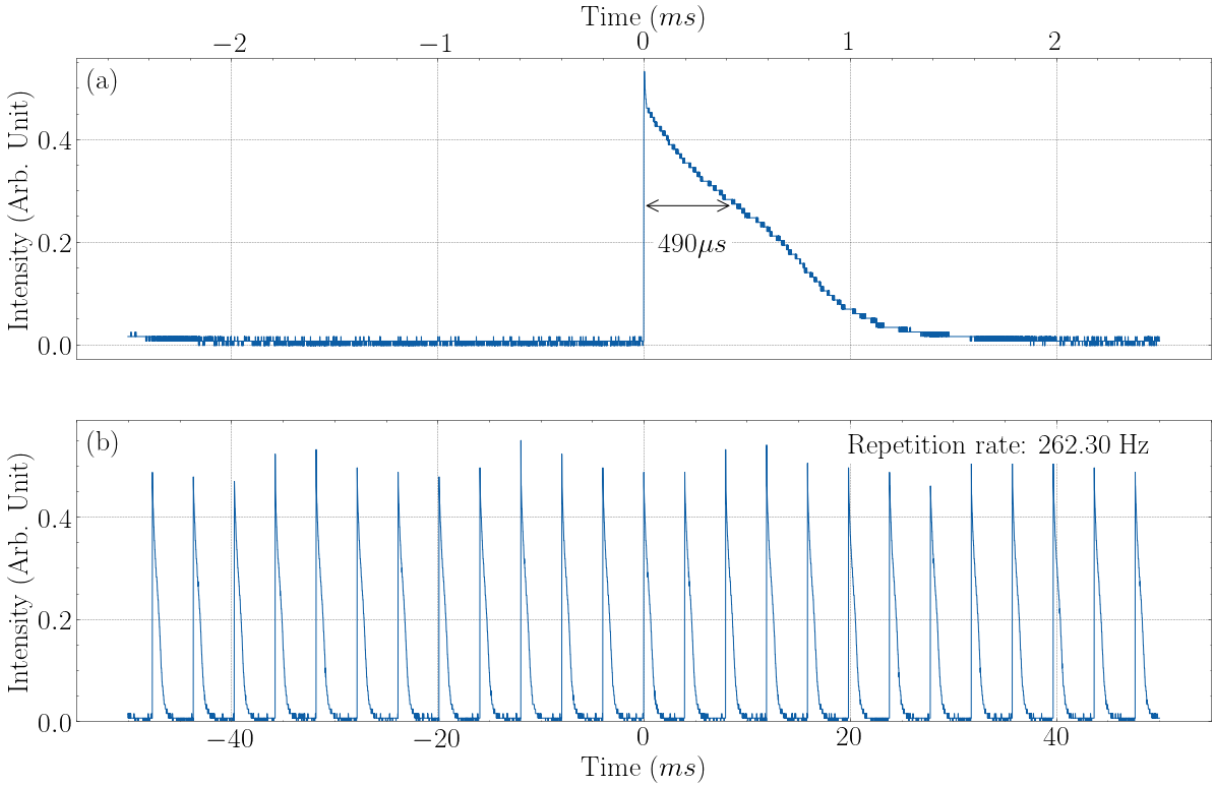

Figure 19. (a) Single Q-switched Nd:YAG laser pulse. (b) pulse train of Q-switched Nd:YAG laser at 262.30 Hz

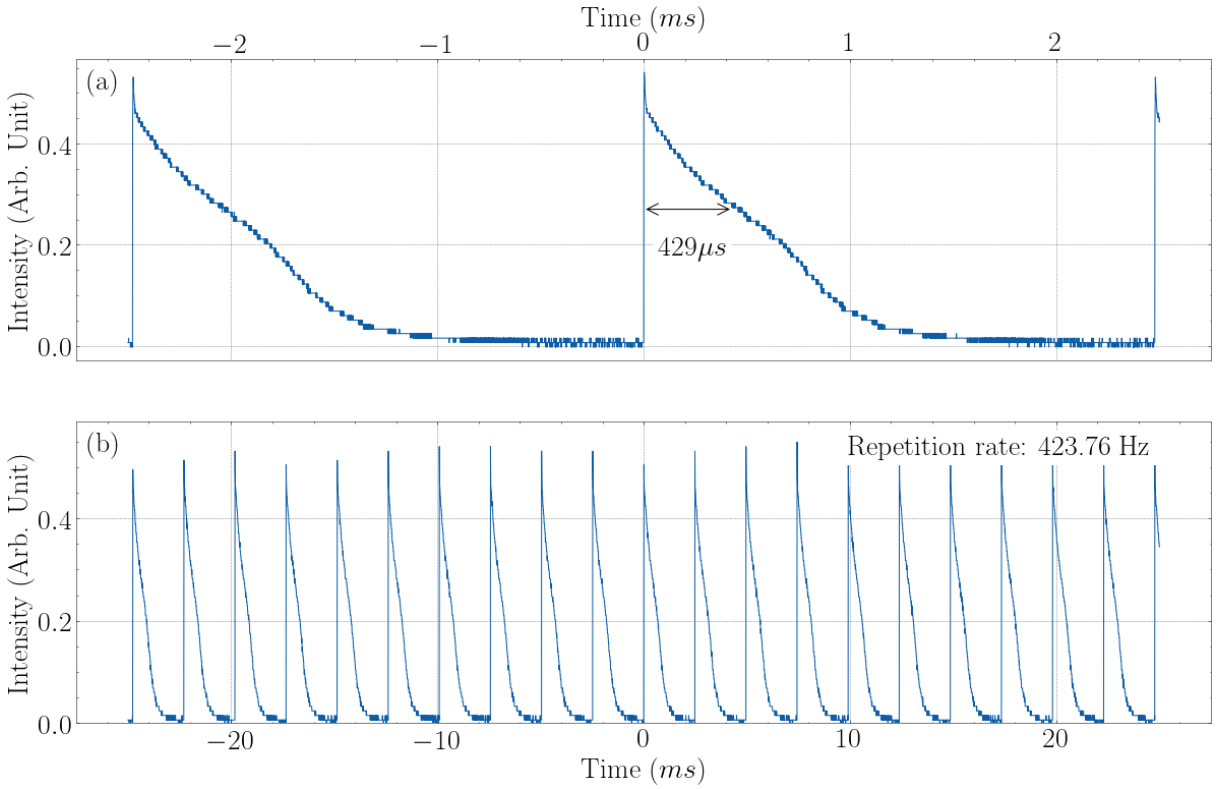

Figure 20. (a) Single Q-switched Nd:YAG laser pulse. (b) pulse train of Q-switched Nd:YAG laser at 423.76 Hz.

Discussion

The Nd:YAG laser system with the diode pump is optimized throughout the experiment and as a result, we are able to generate meaningful data over a long range of values. The pump power of the diode laser as a function of diode current shows a positively correlated linear relationship with relatively mean square residuals. It is expected that, as current is increased, provided temperature variation is small (<3°C), the output power will increase as well. An increased current in the diode indicates more excited charge carriers are being introduced to the system, therefore increasing the probability of stimulated emission and generating larger lasing power.

Same relationship also applies to the output power of the Nd:YAG laser as a function of diode power in that it is roughly a positively correlated linear one with observable deviations when the pump power is in the 100-250 mW range. One can explain these deviations from not only intrinsic experimental errors, but also the fact that pump power is not directly measured but rather an interpretation using the linear fit of our data in figure 12. One can observe that the data points when the pump power is in the 100-250 mW range in figure 12 also shows more visible deviations from the fitted line when compared to the rest of the data points.

Intracavity power in the continuous wave mode is also calculated by assuming 2% transmission for output mirror at 1064 nm wavelength. Calculated intracavity power as a function of diode pump power for 0% to 10% losses are shown in Figure 14.

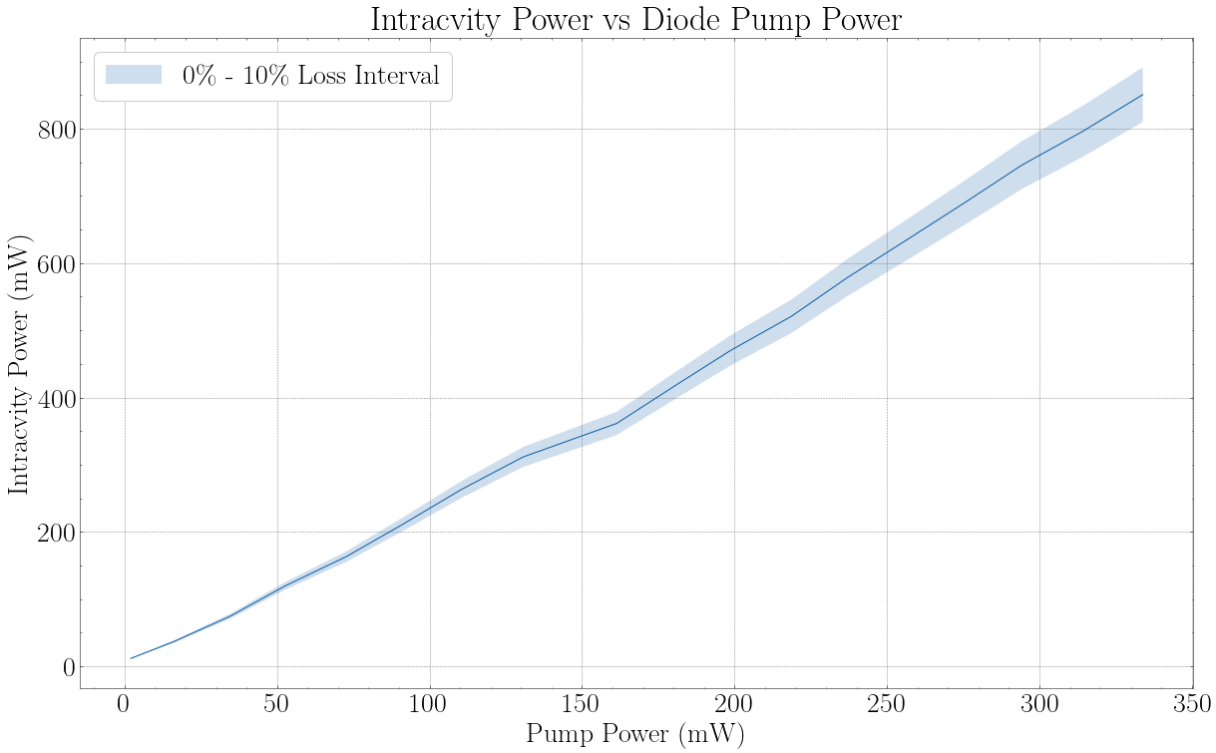

Figure 21. Calculated intracavity power at 1064 nm as a function of pump power.

When the diode current is maintained at 500mA and diode temperature is gradually increased from 10 to 40 °C, the output power of the Nd:YAG laser first increased exponentially from 10 to 20°C, then a logarithm like increase is observed till the output power peaked at 30 °C, and it decreased as temperature is increased till 40 °C. We would like to attribute this behavior to the temperature dependence of a semiconductor's bandgap. In most cases, the energy gap

between the valence band and conduction band will decrease with increasing temperature, decreasing a semiconductor's resistivity as well. When the band gap is larger at lower temperature, the photons emitted when electrons and holes recombine radiatively will have a larger energy as well, and vice versa for photons emitted when the band gap becomes smaller at elevated temperature. Since the pumping medium is made from a pn junction with a GaAs active zone where emission happens, its bandgap essentially determines the wavelength of the photon emitted from the pump. If the bandgap is too large at low temperatures, photons emitted will have excess energy that will be lost when promoting stimulated emission of the Nd:YAG laser. Only when the diode is at optimized bandgap that is compatible for the four-level system of the Nd:YAG laser is then power output also maximized at constant current. As the bandgap gradually decreases, photons emitted become less likely to promote stimulated absorption and achieving population inversion due to the mismatch of photon energy and energy gap of the Nd:YAG levels. Therefore, we observed an increase of pump power as temperature is increased, peaking at optimized wavelength region for pumping the Nd:YAG laser, then decreased as the temperature increased even more.

We have successfully observed the generation of second harmonics as we detected power output of the second harmonic at 532nm. Quadratic relation of second harmonic power as a function of fundamental wave is observed in figure 22, which is in good agreement with theoretical prediction according to equation 10. To induce a significant generation of second harmonics, the KTP crystal was placed in the intracavity configuration. The high electric field strength inside of the cavity is preferable because higher order nonlinear susceptibilities in most dielectric media is small.

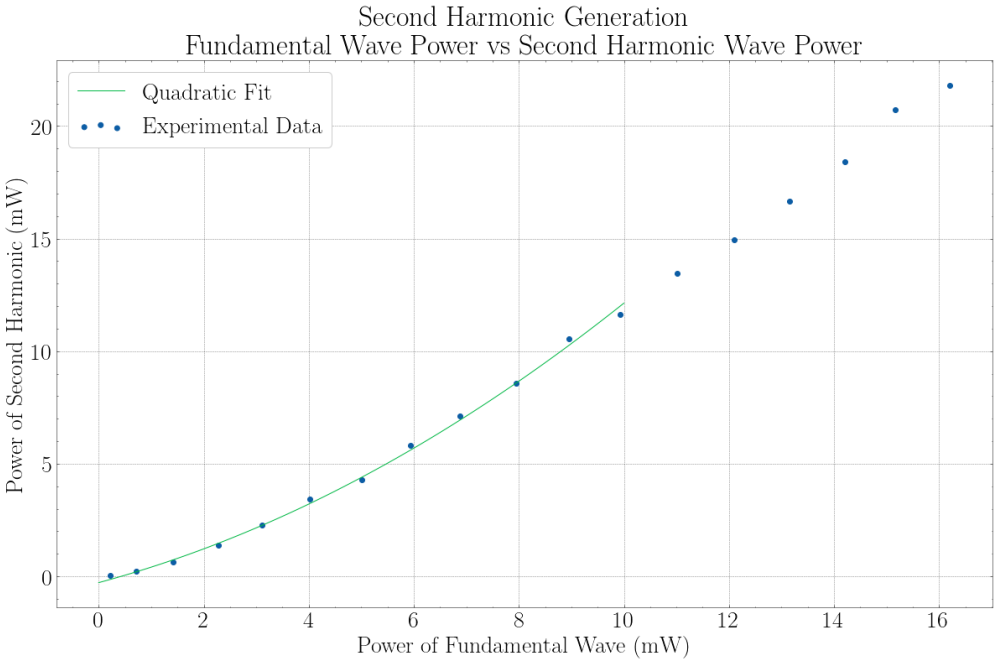

Figure 22. Second harmonic power vs fundamental wave power in near position.

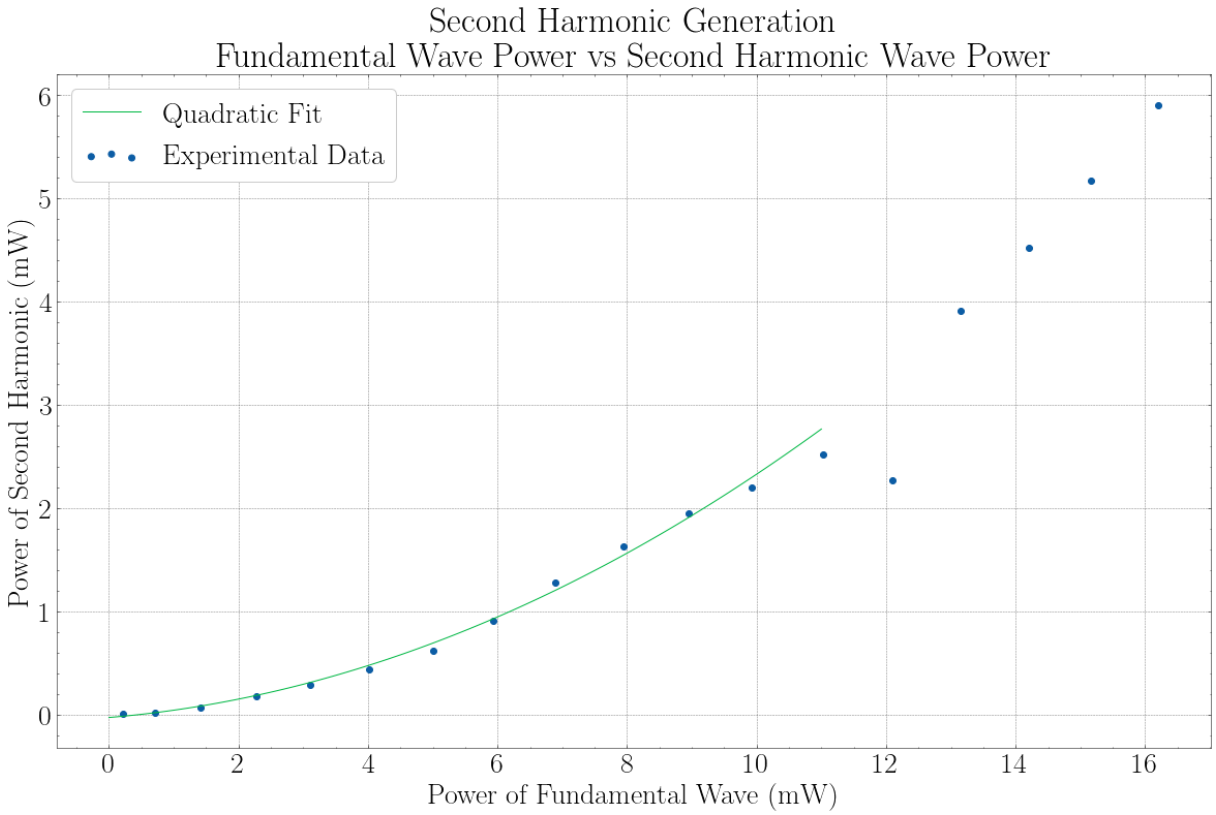

Figure 23. Second harmonic power vs fundamental wave power in far position.

Using the intracavity power calculated with fundamental wave, intracavity power conversion efficiency is calculated for the near and far position of KTP (Figure 24).

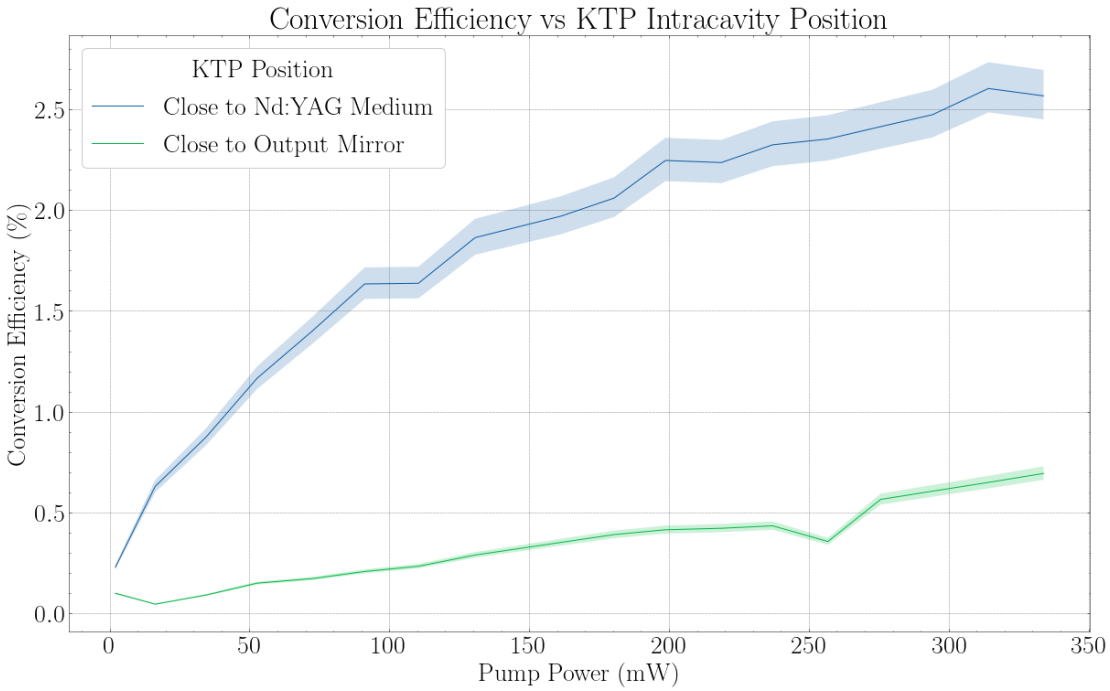

Figure 24. Second harmonic conversion efficiency as a function of pump power for two different positions of the KTP crystal in optical cavity.

The conversion efficiency across the board for the near position is higher than that of the far position. This is a result of the shape of the light envelop being not uniform inside of an

hemispherical optical cavity in our experimental set up with radius of the first mirror equals to 10cm, and radius of the second mirror approaching infinity (Figure 25.) When KTP crystal is placed in the near position, the field strength is much larger than when the KTP is placed in the far position, therefore able to generate second harmonics much more efficiently especially at high pump power (Figure 24).

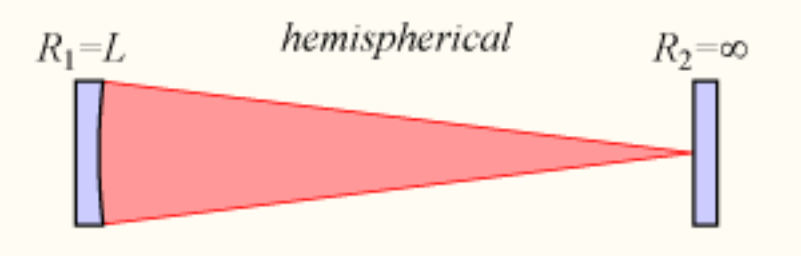

Figure 25. Radiation pattern inside of a hemispherical optical cavity [7].

When the Nd:YAG laser is operated in the Q switching mode with intracavity second harmonic generation, we successfully observed pulsing of the green light at various frequencies. Individual pulses have clearly asymmetric rising and falling edges due to the difference in the rate at which lasing is built up after the opening of the Q switch and the depletion rate.

We calculated more accurate frequencies from the oscilloscope data and it is determined to be 103.46Hz, 263.30Hz, and 423.76Hz. Pulse energy $446.65\ nJ$ is calculated by multiplying period of pulse $9.67\ ms$ and average power $46.21\ \mu W$. Integrating area over single pulse corresponded to pulse energy 0.28 arbitrary unit(a.u.) times micro second. Equating pulse energy For KTP laser to the area under the pulse, one arbitrary unit is determined to be $1.59\ mW$. Therefore, peak power of the pulse at $0.55\ a.u.$ corresponds to 0.87mW.

Using the same calculations, peak power of pulses of frequencies at around ~250 Hz and 400 Hz are calculated. Taking background power detected at 506.2nW into consideration, other characteristics of the Q-switched Nd:YAG laser pulse are also determined and tabulated in Table 2. All of these results exhibit little to no dependence on the modulation frequency, which we attribute to the short lifetime of the metastable levels, as well as a rapid population inversion and saturation of the active medium due to the high pumping power – both processes occurring on timescales significantly shorter than the modulation frequency.

Rise Time	$1.066\ ns \pm 0.301\ ns$
Fall Time	$1.045\ ms\ \pm 0.059\ ms$
$\boldsymbol{T_{FWHM}}$	$452.67\ \mu s\ \pm 26.72\ \mu s$
Pulse Energy	$434\ nJ\ \pm 8\ nJ$
Peak Power	$0.9\ mW \pm 0.1\ mW$

Table 2. Characteristic values for the Q-switched Nd:YAG laser

Conclusion

In this experiment, fundamental properties of the diode laser as a pump laser and the Nd:YAG solid-state laser were studied and characterized. Both the diode pump and the Nd:YAG laser was well optimized throughout the experiment. We observed a linear dependence of the output power of the diode laser to the diode current, as well as a linear dependence of the output power of the Nd:YAG laser to the diode pump power. When diode current was maintained constant and temperature of the diode was varied, a more complicated, non-linear correlation was documented, which we attributed to the shortening of bandgap in a semiconductor, that resulted in optimal conversion efficiency at a temperature between 28 to 31°C. Generation of the second harmonics were observed and a quadratic relationship between the power of the second harmonic and the fundamental was characterized. We have also observed discrepancies in the conversion efficiency of the second harmonic when KTP crystal was placed at two difference positions inside of the cavity due to the asymmetric radiation pattern inside of a hemispherical optical cavity used in our experiment. Lastly, a pulsed lasing mode was realized through a Pockels cell and Q-switching. Through studying the pulse trains at various modulation frequencies, we were able to obtain meaningful information such as pulse energy and peak power of our laser system.

References:

[1] E. Hecht, *Optics*, Revised edition. Boston: ADDISON WESLEY PUB CO INC, 2016.
[2] "MA 14: Solid State Laser Principles." Freie Universität Department of Physics.
[3] Gabriel O'Brien, "Chapter 4b," 12:09:36 UTC. Accessed: Jun. 20, 2022. [Online]. Available: https://www.slideshare.net/chinkitkit/chapter-4b
[4] P. A. Franken, A. E. Hill, C. W. Peters, and G. Weinreich, "Generation of Optical Harmonics," *Phys. Rev. Lett.*, vol. 7, no. 4, pp. 118–119, Aug. 1961, doi: 10.1103/PhysRevLett.7.118.
[5] D. R. Paschotta, "Frequency Doubling." https://www.rp-photonics.com/frequency_doubling.html (accessed Jun. 20, 2022).
[6] "Phase Matching for Nonlinear Optical Processes," *Fosco Connect*. https://www.fiberoptics4sale.com/blogs/wave-optics/phase-matching-for-nonlinear-optical-processes (accessed Jun. 20, 2022).
[7] G. Dattoli, D. Mario, M. Labat, P. Ottaviani, and S. Pagnutti, "Introduction to the Physics of Free Electron Laser and Comparison with Conventional Laser Sources," Oct. 2010, doi: 10.5772/35429.